energies

MDPI

Article

Degradation Prediction and Cost Optimization of Second-Life Battery Used for Energy Arbitrage and Peak-Shaving in an Electric Grid

Rongheng Li, Ali Hassan, Nishad Gupte, Wencong Su and Xuan Zhou *

Department of Electrical and Computer Engineering, University of Michigan-Dearborn, Dearborn, MI 48128, USA; rongheng@umich.edu (R.L.); alihssn@umich.edu (A.H.); nishadg@umich.edu (N.G.); wencong@umich.edu (W.S.)
* Correspondence: xuanzhou@umich.edu

Abstract: With the development of the electric vehicle industry, the number of batteries that are retired from vehicles is increasing rapidly, which raises critical environmental and waste issues. Second-life batteries recycled from automobiles have eighty percent of the capacity, which is a potential solution for the electricity grid application. To utilize the second-life batteries efficiently, an accurate estimation of their performance becomes a crucial portion of the optimization of cost-effectiveness. Nonetheless, few works focus on the modeling of the applications of second-life batteries. In this work, a general methodology is presented for the performance modeling and degradation prediction of second-life batteries applied in electric grid systems. The proposed method couples an electrochemical model of the battery performance, a state of health estimation method, and a revenue maximization algorithm for the application in the electric grid. The degradation of the battery is predicted under distinct charging and discharging rates. The results show that the degradation of the batteries can be slowed down, which is achieved by connecting numbers of batteries together in parallel to provide the same amount of required power. Many works aim for optimization of the operation of fresh Battery Energy Storage Systems (BESS). However, few works focus on the second-life battery applications. In this work, we present a trade-off between the revenue of the second-life battery and the service life while utilizing the battery for distinct operational strategies, i.e., arbitrage and peak shaving against Michigan's DTE electricity utility's Dynamic Peak Pricing (DPP) and Time of Use (TOU) tariffs. Results from case studies show that arbitrage against the TOU tariff in summer is the best choice due to its longer battery service life under the same power requirement. With the number of retired batteries set to increase over the next 10 years, this will give insight to the retired battery owners/procurers on how to increase the profitability, while making a circular economy of EV batteries more sustainable.

Keywords: second-life battery; electricity grid application; electrochemical modeling; degradation prediction; battery operational strategy

Citation: Li, R.; Hassan, A.; Gupte, N.; Su, W.; Zhou, X. Degradation Prediction and Cost Optimization of Second-Life Battery Used for Energy Arbitrage and Peak-Shaving in an Electric Grid. *Energies* **2023**, *16*, 6200. https://doi.org/10.3390/en16176200

Academic Editor: Simone Barcellona

Received: 31 July 2023
Revised: 19 August 2023
Accepted: 21 August 2023
Published: 26 August 2023

1. Introduction

With the widespread use of electric vehicles, huge numbers of batteries are employed. As the battery is charged and discharged continuously, the capacity degrades gradually. When it reaches a certain level, i.e., 80% of the original state of health, the battery should be retired from the electric vehicles [1,2]. With the continuous development of the electric vehicle industry, the number of batteries retired from vehicles is increasing rapidly. The expense of disassembling and recycling these batteries is relatively high, which raises a substantial issue on how to handle them appropriately. A recent work that utilizes an indicator, i.e., global warming potential, demonstrates that reusing the existing electric vehicle battery in a secondary application provides a significant environmental benefit compared to manufacturing a new battery for the same purpose [3]. By appropriate assessment and treatment, the retired batteries can be utilized for other applications. Such

reused batteries are referred to as second-life batteries [4–6]. The implementation of second-life batteries is also beneficial for protecting the environment and saving money [7].

Among the various applications of the second-life battery, it is found to be suitable for employment as an energy storage system in the electricity grid system [8]. Energy storage systems have proven to be a game changer for the integration of renewable energy and the stability of modern power systems [9]. Their use in the grid can be for various purposes. In [10], G. Fitzgerald et al. mentioned thirteen different uses for BESSs in general. Main grid utilization of BESSs is for energy arbitrage [11–13], frequency regulation [14–16], peak shaving [17–19], or power smoothing [20–22]. The second-life batteries have been deployed by industrial consortiums as discussed in [23–25]. In [26], Zhang et al. proposes a remaining useful life prediction methodology using a deep learning integrated approach. In [27], Xiofan et al. discusses a power processing methodology for power converters for power optimization of second-life batteries. Many research studies [28–30] focus on the aging of a fresh energy storage system, however, there is a clear research gap in predicting the degradation of second-life batteries. Therefore, accurate battery performance estimation becomes essential in the choice of operational grid strategies. In the short-term range, correct estimation of the battery charging and discharging responses can enhance the stabilization of the grid system [31]. For the long-term consideration, accurate state of health prediction of the second-life battery is beneficial for reducing the cost and improving the grid system efficiency [32].

For distinct working conditions, i.e., operational strategies and user loads, the cost-effectiveness of the batteries can be optimized with appropriate configurations, i.e., series and parallel connections [33]. Compared to costly and time-consuming experimental testing, numerical modeling is a better approach to speed up the simulation of the operating process [34]. The three main categories of modeling methods are the physics-based electrochemical models [35], the electrical equivalent circuit models [36,37], and the data-driven models [38,39]. The advantages and limitations of these approaches are summarized in Table 1. The physics-based model shows the mechanisms of electrochemical reactions, which are particularly important in predicting degradation. Among various models, the Doyle-Fuller-Newman (DFN) model attracts great attention due to its good accuracy and suitability for diverse working conditions [40]. For engineering practice, the P2D model is simplified to a more concise form [41,42]. Xu et al. presented an electrochemical-thermal-capacity model that minimizes capacity fade and reduces the temperature rise to prevent a thermal runaway [43]. Song et al. developed an electro-chemo-mechanical model, which couples the mechanical and electrochemical factors [44]. The framework of the P2D model is implemented in commercial software, such as COMSOL [45], and open-source codes, i.e., DUALFOIL [46], LIONSIMBA [47], and PyBaMM [48].

Table 1. A summary of the battery performance modeling approaches, including their benefits and limitations.

Category	Benefits	Limitations
Physics-based electrochemical models [35,40–43]	Reveal the physical phenomenon behind the battery; suitable for wide scenario ranges	Complex to implement; time-consuming
Electrical equivalent circuit models [36,37]	Robust; easy to implement	Less accurate
Data-driven models [38,39]	Moderate accuracy; knowledge of the underlying process is not required	Accuracy depends on the quality of training data; usually requires a large set of charging and discharging data

A number of major degradation mechanisms are proposed to accurately model the battery aging process. They are solid electrolyte interphase (SEI) layer growth, lithium plating,

particle cracking, and active material losses. Safri et al. developed a solvent-decomposition reaction model to simulate the growth of solid electrolyte interphase at the anode [49]. Single et al. revealed the mechanism of SEI formation [50]. Their work demonstrated that the diffusion of neutral radicals is the cause of long-term SEI growth. Luo et al. revealed the mechanism of SEI formation [51]. They simulated the battery degradation under various depths of discharge, state-of-charge swing ranges, and temperatures. O'Kane et al. coupled four degradation mechanisms in the electrochemical model [52]. They reported that five distinct pathways can result in end-of-life, which depends on how the cell is charged and discharged.

This article outlines a technique for predicting the performance and degradation of second-life batteries utilized in electric grid systems. The approach consists of an electrochemical model of the battery's performance, a health monitoring method, and an algorithm to reduce costs for grid applications. The governing equations of the electrochemical process and the degradation mechanisms are demonstrated. Different charging and discharging rates are utilized to predict battery degradation. The study shows that the connection of batteries in parallel can slow down the degradation, but this option requires a balance between the cost of the battery and its lifetime. Different charging and discharging strategies are considered in the research, including DPP and TOU. The strategy with both a longer battery life and mediate cost is depicted.

The main contributions of this work are summarized as follows:

- A methodology that couples the DFN electrochemical model and a revenue maximization algorithm is introduced to model the performance of a second-life battery in the application of the electric grid.
- Simulations of distinct configurations demonstrate that a trade-off between the revenue of the battery and the service life should be optimized.
- Through the implementation of distinct battery operational strategies, the study illustrates that the arbitrage against the TOU tariff in summer is the optimal solution among various combinations due to its longer battery service life while providing the same amount of power.

2. Methodology

The structure of a battery under the P2D model configuration is displayed in Figure 1. The cell consists of three regions: the positive electrode, the separator, and the negative electrode. The active materials are modeled as spherical particles that fill in the positive and negative electrodes. Two dimensions are considered in the P2D model. The x-axis is defined in the direction perpendicular to these layers to account for the diffusion and migration of Li ions in the liquid phase. The origin of the *r*-axis is at the center of the solid sphere, which describes the diffusion of Li ions in the active materials.

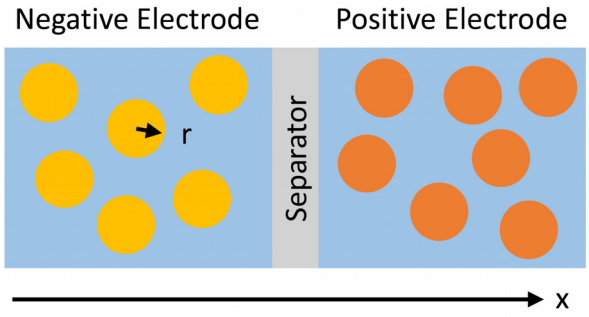

Figure 1. Structure configuration of the P2D model of the Li-ion battery.

2.1. P2D Models

The electrochemical process described in P2D models is governed by the following five partial differential equations. They are the equations for: charge conservation in the homogeneous solid, mass conservation in the homogeneous solid, mass conservation in the

homogeneous electrolyte, charge conservation in the homogeneous electrolyte, and lithium movement between the solid and electrolyte phases [40,53,54].

2.1.1. Mass Conservation in Solid

The lithium diffusion inside the solid particles is driven by the gradient of its concentration, which is governed by Fick's second law as:

$$\frac{\partial c_s(x,r,t)}{\partial t} = \frac{1}{r^2}\frac{\partial}{\partial r}\left(D_s r^2 \frac{\partial c_s\,(x,r,t)}{\partial r}\right) \tag{1}$$

where $c_s(x,t,r)$ and D_s are the concentration and the diffusion coefficient of lithium in the solid phase, respectively. The initial condition is:

$$c_s(x,r,t)|t\ = 0\ = C_{s,0} \tag{2}$$

The boundary conditions are:

$$D_s \left.\frac{\partial c_s\,(x,r,t)}{\partial r}\right|_{r=0} = 0 \tag{3}$$

$$D_s \left.\frac{\partial c_s\,(x,r,t)}{\partial r}\right|_{r=R_s} = \frac{j(x,t)}{F} \tag{4}$$

where $c_{s,0}$, R_s, F, and $j(x,t)$ are the initial concentration of lithium, the radius of solid-state particles, the Faraday constant, and the current density of the surface particle's electrochemical reaction rate, respectively.

2.1.2. Mass Conservation in Electrolyte

The movement of lithium ions inside the electrolyte is governed by the diffusion and migration process, which is described by:

$$\varepsilon_e \frac{\partial c_e(x,t)}{\partial_t} = \frac{\partial}{\partial x}\left(D_e^{eff}\frac{\partial c_e(x,t)}{\partial_x}\right) + a_s\left(1-t_+^0\right)\frac{j(x,t)}{F} \tag{5}$$

with $c_e(x,t)$, ε_e, and t_+^0 being the lithium ion concentration, the electrolyte volume fraction, and the lithium ion transfer number, respectively. D_e^{eff} is the effective diffusion coefficient in the electrolyte and is expressed as:

$$D_e^{eff} = \varepsilon_e^{brugg} D_e \tag{6}$$

where ε_e^{brugg} is the Bruggeman correction coefficient. D_e is the electrolyte diffusion coefficient. The specific surface area of the solid particles is calculated as:

$$a_s = \frac{3\varepsilon_s}{R_s} \tag{7}$$

where ε_s is the solid phase volume fraction.

The corresponding boundary conditions are:

$$\left.\frac{\partial c_e(x,t)}{\partial_x}\right|_{x=0} = \left.\frac{\partial c_e(x,t)}{\partial_x}\right|_{x=L} = 0 \tag{8}$$

$$D_{e,neg}^{eff}\left.\frac{\partial c_e(x,t)}{\partial_x}\right|_{x=x_{neg}} = D_{e,sep}^{eff}\left.\frac{\partial c_e(x,t)}{\partial_x}\right|_{x=x_{neg}^+} \tag{9}$$

$$c_e(x,t)|_{x=x_{neg}^-} = c_e(x,t)|_{x=x_{neg}^+} \tag{10}$$

$$D_{e,sep}^{eff}\frac{\partial c_e(x,t)}{\partial_x}\bigg|_{x=x_{sep}} = D_{e,pos}^{eff}\frac{\partial c_e(x,t)}{\partial_x}\bigg|_{x=x_{sep}^{+}} \tag{11}$$

$$c_e(x,t)|_{x=x_{sep}^{-}} = c_e(x,t)|_{x=x_{sep}^{+}} \tag{12}$$

where $x = 0$ represents the boundary between the current collector and the negative electrode; $x = x_{neg}$ is the boundary between the negative electrode and the separator; $x = x_{sep}$ defines the boundary between the separator and the positive electrode. In addition, the superscripts "−" and "+" denote the negative and positive portions of the battery.

2.1.3. Charge Conservation in Solid

Charge conservation shows that there is rarely a loss of net charge. Ohm's law can be seen in the electrode solid-phase potential distribution, which can be stated as follows:

$$-\frac{\partial i_s(x,t)}{\partial x} = \frac{\partial}{\partial x}\left(\sigma_s^{eff}\frac{\partial}{\partial x}\varnothing_s(x,t)\right) = a_s j(x,t) \tag{13}$$

where $i_s(x,t)$ is the electrical current density in the solid phase, $\phi_s(x,t)$ is the potential present in the solid phase, and σ_S^{eff} is the material's effective electrical conductivity in the solid state defined as:

$$\sigma_S^{eff} = \varepsilon_s^{bu}\sigma_s \tag{14}$$

with σ_s denoting the material's conductivity in the solid phase.

The boundary conditions are as follows:

$$-\sigma_s^{eff}\frac{\partial}{\partial x}\varnothing_s(x,t)\bigg|_{x=0} = -\sigma_s^{eff}\frac{\partial}{\partial x}\varnothing_s(x,t)\bigg|_{x=L} = \frac{I_{app}(t)}{A_{cell}} \tag{15}$$

where cell A is the electrode area and $I_{app}(t)$ is the charge/discharge current value of the external circuit when the battery is functioning.

2.1.4. Charge Conservation in Electrolyte

The change is conserved in the liquid phase. The lithium ions are intercalated and deintercalated inside the solid particles, which is governed by:

$$-\frac{\partial i_e(x,t)}{\partial x} = \frac{\partial}{\partial x}\left(k_e^{eff}\frac{\partial}{\partial x}\varnothing_e(x,t)\right) + \frac{\partial}{\partial x}\left(k_D^{eff}\frac{\partial}{\partial x}lnc_e(x,t)\right) = -a_s j(x,t) \tag{16}$$

where $i_e\ (x,t)$, $c_e(x,t)$, $\phi_e(x,t)$, and k_e^{eff} are the ionic current density, the lithium concentration, the potential, and the effective ionic conductivity in the electrolyte. Then:

$$k_e^{eff} = \varepsilon_e^{brugg}K_e \tag{17}$$

with K_e being the ionic conductivity of the electrolyte. The effective diffusion conductivity of the electrolyte is expressed as:

$$k_D^{eff} = \frac{2RTk_e^{eff}}{F}(1 + \frac{d\ lnf_{\pm}}{d\ lnc_e})(t_+^0 - 1) \tag{18}$$

with R, T, and $f_{\pm}$ being the gas constant, the temperature, and the molar activity coefficients of the electrolyte. The boundary conditions are:

$$\frac{\partial\varnothing_e(x,t)}{\partial_x}\bigg|_{x=0} = \frac{\partial\varnothing_e(x,t)}{\partial_x}\bigg|_{x=L} = 0 \tag{19}$$

$$i_e(x,t)|_{x=x_{neg}^-} = i_e(x,t)|_{x=x_{neg}^+} = \frac{I_{app}\ (t)}{A_{cell}} \tag{20}$$

$$\varnothing_e(x,t)|_{x=x_{neg}^-} = \varnothing_e(x,t)|_{x=x_{neg}^+} \tag{21}$$

$$i_e(x,t)|_{x=x_{sep}^-} = i_e(x,t)|_{x=x_{sep}^+} = \frac{I_{app}\ (t)}{A_{cell}} \tag{22}$$

$$\varnothing_e(x,t)|_{x=x_{sep}^-} = \varnothing_e(x,t)|_{x=x_{sep}^+} \tag{23}$$

2.1.5. Electrochemical Kinetics Equation

To link the surface over potential $\eta(x,t)$ with the electrochemical reaction rate $j(x,t)$, the Bulter–Volmer kinetic equation is employed.

$$j(x,t) = i_0\left[exp\left(\frac{\alpha_a F}{RT}\eta(x,t)\right) - exp\left(\frac{-\alpha_c F}{RT}\eta(x,t)\right)\right] \tag{24}$$

with i_0, α_a, and α_c being the exchange current density, the transfer coefficient of the anode, and the transfer coefficient of the cathode, respectively. The overpotential is expressed as:

$$\eta(x,t) = \varnothing_s(x,t) - \varnothing_e(x,t) - E_j^{ref}(\theta_j(x,t)) - j(x,t)R_{SEI} \tag{25}$$

with R_{SEI} being the resistance of the SEI film, and E_j^{ref} being the equilibrium potential of the electrodes. In addition:

$$\theta_j(x,t) = \frac{c_{s,surf(x,t)}}{c_{s,max,j}}, j = neg, pos \tag{26}$$

where $c_{s,surf}\ (x,t)$ stands for the lithium concentration of the active material surface; $c_{s,\ max}$ is the maximal lithium concentration of electrodes. The exchange current can be calculated as:

$$i_0 = Fk_0\left(c_{s,max} - c_{s,surf}\right)^{\alpha_a} {c_{s,surf}}^{\alpha_c} {c_e}^{\alpha_a} \tag{27}$$

with k_0 as the electrochemical reaction rate constant.

2.2. State of Health

For the long-term lifespan, four mechanisms can be utilized for the prediction of the state of health. In this paper, the interstitial-diffusion-limited SEI growth model is implemented [51]. The four mechanisms are the solid electrolyte interphase layer growth, lithium plating, particle cracking, and active material losses.

$$j_{inter}^* = -\frac{F^* D_{Li,i}^*}{L_\sigma^*} c_{Li,i,0}^* \exp\left(-\frac{F^*}{R_g^* T^*}(\varnothing_{s,n}^* - \varnothing_{s,e}^*)\right) \tag{28}$$

Here, j_{inter}^* represents the interfacial current density, $D_{Li,i}^*$ is the diffusivity of lithium ions in the inner SEI, $\varnothing_{s,n}^*$ is the negative electrode potential, and $c_{Li,i,0}^*$ is the inner SEI's concentration of lithium ion interstitials when $\varnothing_{s,n}^* = \varnothing_{e,n}^*$. Here, $\varnothing_{e,n}^*$ is the true electrolyte potential, F^* shows Faraday's constant, R_g^* is the universal gas constant, and T^* is the reference temperature. The lithium plating is considered irreversible in this work. For the lithium plating portion, the irreversible model is selected. The SEI on cracks and loss of active material losses are not considered in this work. The description and derivation of the governing equations for the degradation mechanisms are well demonstrated in [48–52,55]. The default settings of PyBaMM are utilized for the rest simulations.

2.3. Grid Optimization

This section will present an optimization problem for the LG M50 cylindrical cell used in a pack acting as an energy storage system to provide power to the grid for two management strategies: energy arbitrage and peak shaving. They are under extensive investigation on the demand side in the area of power systems. Arbitrage involves exploiting temporal price variations in the electricity market by purchasing electricity during periods of lower prices and selling it during periods of higher prices, thereby maximizing economic gains. On the other hand, peak shaving aims to strategically decrease electricity consumption during peak demand periods to smooth out load curves and reduce grid stress. The advancement of sustainable energy systems is aided by these strategies, which play a crucial role in enhancing grid stability, cost-effectiveness, and the integration of renewable energy sources.

The mathematical statement of the optimization problem is described in the following equations.

$$max \sum_{t=1}^{96} E_{dch}(t) C_{pk}(t) - E_{ch}(t) C_{ofpk}(t) \tag{29}$$

s.t.

$$C_{battery}(t) = C_{battery}(t-1) + E_{ch}(t)\eta_{ch} - E_{dch}(t)\eta_{dch} \tag{30}$$

$$SOC(t=1) = SOC(t=96) \tag{31}$$

$$E_{ch}(t) \leq E_{ch\_max}(t) * 0.95 * u(t) \; \forall u \in 0,1 \tag{32}$$

$$E_{dch}(t) \leq E_{dch\_max}(t) * 0.95 * u(t) \; \forall u \in 0,1 \tag{33}$$

$$SOC_{min} \leq SOC \leq SOC_{max} \tag{34}$$

$$E_{dch}(t) * u(t) + E_{ch}(t) * (1 - u(t)) = 0$$
$$where \begin{cases} u(t) = 1, \; t = 44 \; to \; 80 \\ u(t) = 0, \; t = 1 \; to \; 43 \; or \; 81 \; to \; 96 \end{cases} \tag{35}$$

In Equation (30), E_{dch} is the discharge energy in kWh from the battery, E_{ch} is the charging energy in kWh into the battery, C_{pk} is the cost of energy in USD/kWh for the peak hours, and C_{ofpk} is the cost of energy in USD/kWh for the off-peak hours, respectively. η_{ch} and η_{dch} are the charge and discharge efficiencies taken as 0.95 (95%). The variable $u(t)$ is a binary variable that makes sure that the battery either charges or discharges at one 15-min time interval. The t represents 15-min intervals in a 24-h period, i.e., ($25 \times 15 = 96$). The cost function maximizes the profit earned by selling the power (revenue) subtracted from the money incurred by charging the battery (cost). Constraint (31) calculates the capacity $C_{battery}$ of the battery at each time step t, i.e., $C_{battery}$ decreases if the battery is discharged or increases if it is charged. Equation (31) sets the state of charge SOC at $t = 1$ at the start of the day equal to the SOC at $t = 96$ at the end of the day. Equations (32)–(34) keep the charge energy, discharge energy, and state of charge within the maximum physical limit of the battery, respectively. Equation (35) is an additional constraint only for the peak-shaving strategy that forces the battery to discharge during the peak demand hours. The optimization problem is an MILP formulated using the abstract model in Pyomo 6.6.0 and solved using the CPLEX optimization solver.

The load profile of Southeast Michigan on a typical weekday is given in Figure 2, which shows the load profile for one day of residential customers in Michigan. The load peaks at around 12 p.m. and dips around 8 p.m. This is known as peak load for which utilities must fire up the peak power plants, which is both expensive and inefficient. However, with

recent advances, energy storage systems can be used to provide the stored power to the grid to meet the peak load, which is known as peak shaving.

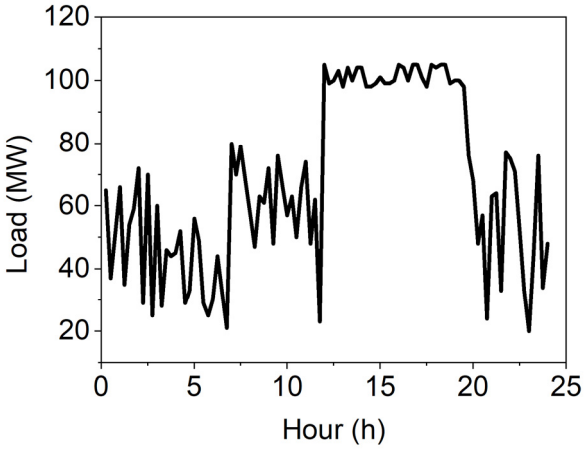

Figure 2. The load profile of Southeast Michigan on a typical weekday.

The optimization problem in this work is solved for the two different residential tariffs of a DTE utility in Michigan: Time of Use (TOU) and Dynamic Peak Pricing (DPP) rate as shown in Table 2. The concept of TOU rate structures is to divide the day into different periods, each with varying electricity prices, which encourages consumers to switch their electricity consumption to off-peak hours when prices are lower. On the other hand, the DPP rate dynamically adjusts electricity prices in real time depending on the supply and demand conditions of the network, favoring a more flexible and reactive consumption behavior.

Table 2. DTE TOU and DPP tariff.

Tariff Type	On-Peak Hours	Mid-Peak Hours	Off-Peak Hours	Summer (Jun through Sep) (₵/kWh (USD))		Summer (Jun through Sep) (₵/kWh (USD))	
				On-Peak	Off-Peak	On-Peak	Off-Peak
Time of Use (TOU)	Monday–Friday 3 p.m. to 7 p.m.	---	Monday–Friday 12 a.m.–3 p.m., 7 p.m.–12 a.m. and all-day Saturday, Sunday	7.941	4.828	5.560	4.828
Dynamic Peak Pricing (DPP)	Monday–Friday 3 p.m. to 7 p.m.	Monday–Friday 7 a.m. to 3 p.m. and 7 p.m. to 11 p.m.	11 p.m. to 7 a.m. and all-day Saturday, Sunday	**Same rates all around the year**			
				On-Peak	**Mid-Peak**	**Off-Peak**	
				12.658	5.486	1.184	

3. Results

3.1. Model Validation

To validate the proposed calculation method, we have conducted simulations using the LG M50 cylindrical cell. The detailed values of battery parameters were taken from the reported works [52,56]. To represent different operating conditions, three distinct discharging rates were selected, which are 0.05C, 1C, and 2C. The voltage responses obtained from our model, which was implemented using PyBaMM v23.5, were compared with experimental data available online and depicted in Figure 3. Due to the significant

difference in discharging timespans between 0.05C and the other rates, their responses were plotted separately in Figure 3a. The model exhibited good agreement with the experimental data for the discharging curve. Minor deviations between simulation results and experimental data were observed for higher discharging rates, i.e., 1C and 2C in Figure 3b, yet remained within acceptable tolerances.

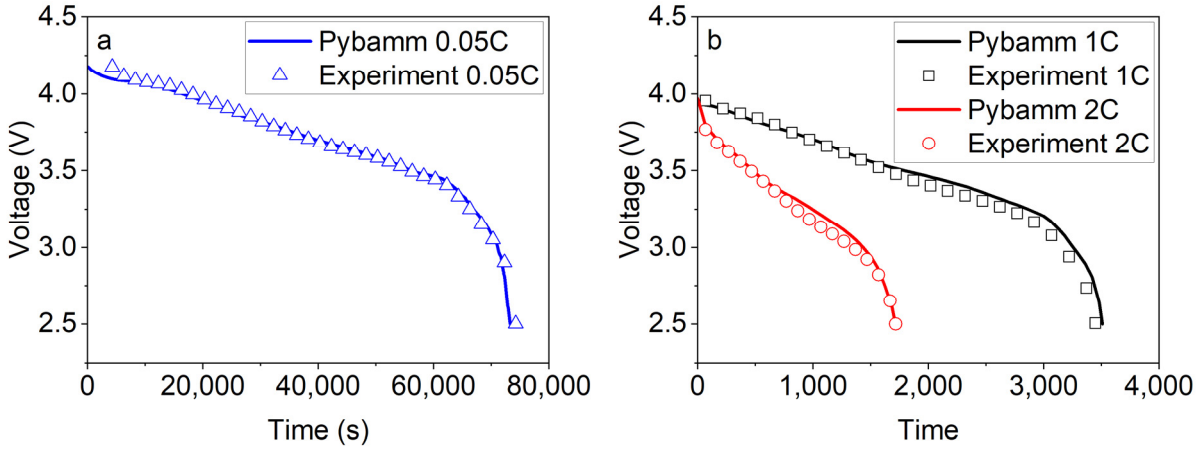

Figure 3. The voltage responses of the battery at (**a**) 0.05C and (**b**) 1C and 2C.

With the short time performance of the battery validated, the long-term degradation estimation is also validated. The following cycling protocol is utilized, which is the same as a testing report. Firstly, the cell is charged at a constant current of 0.33C to 4.2 V. Then, the cell is discharged at the same constant rate of 2.85 V. The above protocol is repeated for 1000 cycles with the discharged capacity displayed in Figure 4. As depicted in the figure, the discharge capacity drops to 4.10 A.h, which is around 80% of the initial capacity. It is well agreed with the reported testing results.

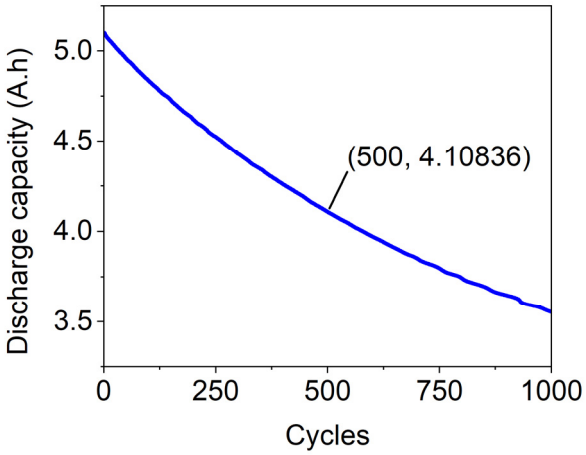

Figure 4. The discharge capacity of the battery for 1000 charging and discharging cycles.

3.2. Optimization for Distinct Strategies

Using the second-life battery cell in a grid would need a scheduled charge and discharge, which is calculated by an optimization problem explained in Section 2. The charge and discharge energy (kWh) of the battery cell is optimized using an optimization problem formulation explained in Section 2.3. while following the constraints. Figure 5a,b shows the charging and discharging energy (kWh) of a battery cell for the DPP tariff for arbitrage and peak-shaving. The battery charges and discharges aggressively for DPP-Arbitrage during hours 8 to 16 while for DPP—Peak-Shaving the charge and discharge trend is concentrated from hours 19 to 22. Likewise, Figure 6a,b show charge and discharge energy

(kWh) calculated for the TOU tariff for summer arbitrage and peak-shaving. Figure 7a,b provides similar results for the TOU tariff for winter. The overall charge and discharge profile is rigorous for TOU summer peak shaving as compared to the rest. In terms of battery degradation, such a profile will lessen cell life. For longer life, the charging and discharging of the battery needs to be less rigorous for TOU peak shaving during winters. The peaks are widely distributed with a uniform discharge during the peak hours.

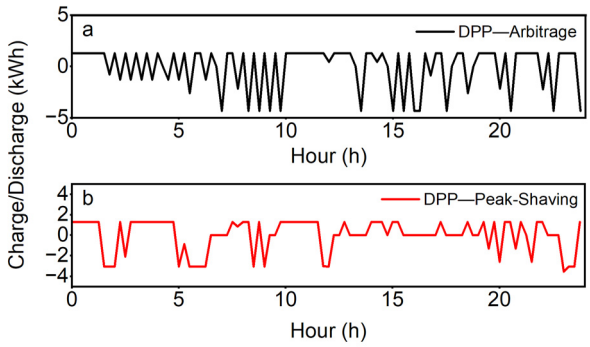

Figure 5. (**a**) Charge and discharge energy (kWh) for arbitrage against DPP tariff; (**b**) charge and discharge energy (kWh) for peak shaving against DPP tariff.

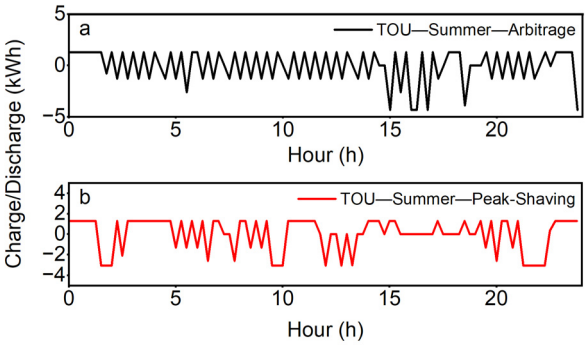

Figure 6. (**a**) Charge and discharge energy (kWh) for arbitrage against TOU tariff (summer); (**b**) charge and discharge energy (kWh) for peak shaving against TOU tariff (summer).

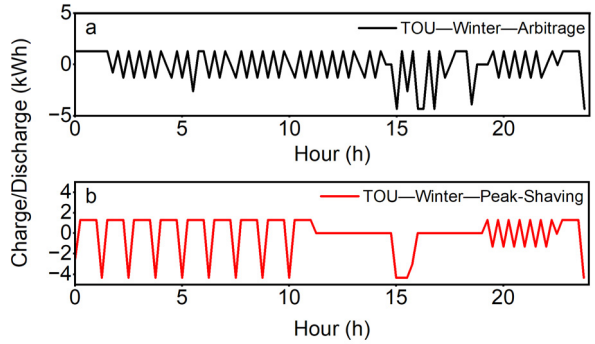

Figure 7. (**a**) Charge and discharge energy (kWh) for arbitrage against TOU tariff (winter); (**b**) charge and discharge energy (kWh) for peak shaving against TOU tariff (winter).

3.3. Battery Cell Capacity

To further expand on the results above, Figures 8–10 show the battery cell's capacity in kWh for DPP and TOU tariffs. Figure 8 shows that the battery capacity profile for DPP peak shaving is more rigorous as compared to DPP arbitrage. For Figure 9, the battery capacity profile for TOU peak shaving in summer is more rigorous than TOU arbitrage in summer. The battery capacity profile for TOU winter peak shaving is more rigorous than

TOU winter arbitrage. Overall, the battery capacity profile for TOU winter arbitrage and peak shaving looks the smoothest as compared to all other cases, which is in accordance with the charge and discharge profile results above.

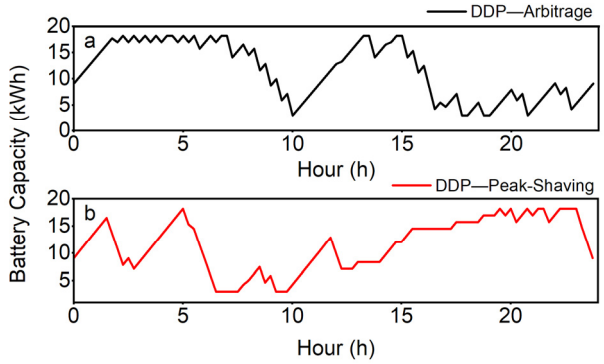

Figure 8. (**a**) Battery capacity (kWh) for 1 day (15 min interval) for DPP arbitrage; (**b**) battery capacity (kWh) for 1 day (15 min interval) for DPP peak shaving.

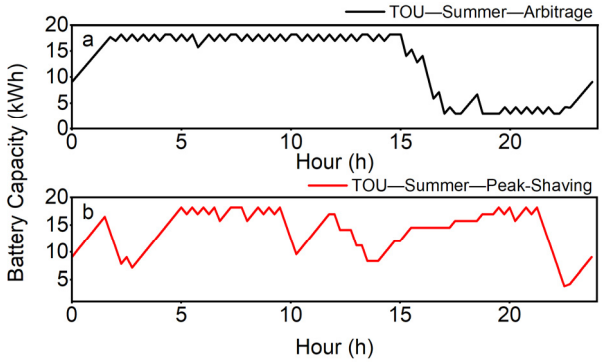

Figure 9. (**a**) Battery capacity (kWh) for 1 day (15 min interval) for TOU (summer) EA; (**b**) battery capacity (kWh) for 1 day (15 min interval) for TOU (summer) peak shaving.

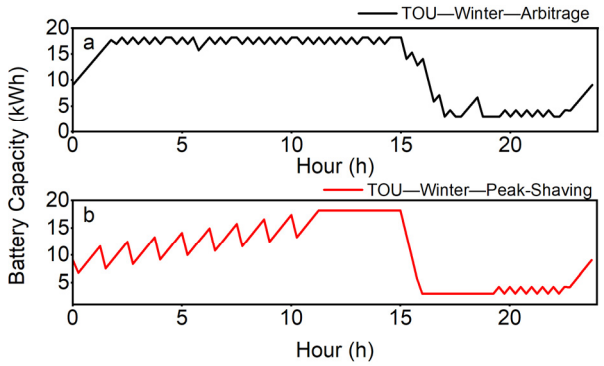

Figure 10. (**a**) Battery capacity (kWh) for 1 day (15 min interval) for TOU (winter) arbitrage; (**b**) battery capacity (kWh) for 1 day (15 min interval) for TOU (winter) peak shaving.

3.4. Usage Days for Different Operational Strategies

In this part, the usage days of two different operational strategies are investigated. Case 1 simulates the configuration in that the required power is supplied using one LG M50 cell, while case 2 is for the same power supplied using two identical cells. For each case, the battery cell(s) starts from 80% of its original state of health, justifying it as a second-life battery use. It will be terminated at 64%, which is 80% of the starting point of the second-life use. Figure 11 shows the cell life (usage days) calculated for two different configurations.

The first configuration considers only one cell providing (discharge) and receiving (charge) energy/power to and from the grid, respectively, against DPP and TOU tariffs for EA and peak shaving. Conversely, the second configuration considers the same for two battery cells. The bar graph shows that cell life is the shortest in the first configuration where the peak shaving is provided by one cell for summer TOU. This is because the cell charges and discharges aggressively for this scenario as compared to the other cases, resulting in heavy cell degradation. The cell life is the longest for the arbitrage case against the DPP tariff. For configuration 2, again the cell life is lowest for peak shaving for TOU (summer), while the cell life is longest for TOU (winter) peak shaving.

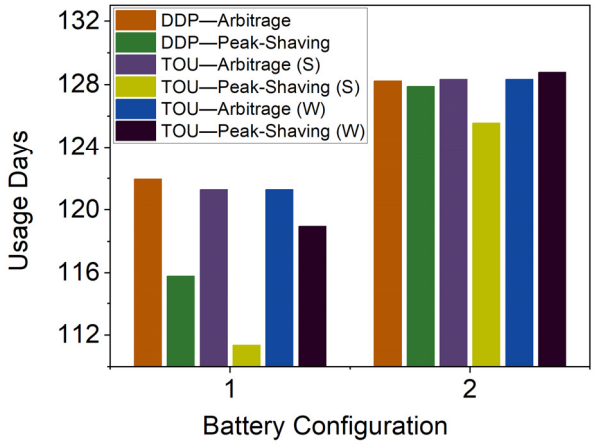

Figure 11. Usage days when required power is provided by one vs. two battery cells.

Table 3 shows the revenue (in USD) calculated by optimizing the cost function. The profit is at a maximum (USD 21.25) for the arbitrage for TOU in summer. However, the degradation for the same battery cell as shown above was the maximum. This again shows that excessive charge and discharge may earn revenue but will also degrade the battery fast. Therefore, the battery needs to generate revenue while at the same time degrading slowly for long life. Considering the results from Figure 11 and Table 3, it is recommended to use the second-life battery pack made of used LG M50 cells for arbitrage against the TOU tariff in summer.

Table 3. DTE TOU and DPP tariff.

Scenario	Profit per 24 h (USD)
DPP—Arbitrage	0.7067
DPP—Peak Shaving	1.77
TOU—Arbitrage (Summer)	20.08
TOU—Peak Shaving (Summer)	21.25
TOU—Arbitrage (Winter)	0.32
TOU—Peak Shaving (Winter)	0.32

4. Conclusions

A method for predicting the performance and deterioration of second-life batteries deployed in electric grid systems is presented in this paper. The approach incorporates an electrochemical model to evaluate battery performance, a health monitoring technique, and a cost-reduction algorithm designed for grid applications. The method predicts battery degradation based on various charging and discharging rates, which reveals that parallel battery connections can mitigate degradation, despite necessitating a balance between battery cost and longevity. Various charging and discharging strategies, including energy arbitrage and peak-shaving against DPP and TOU tariffs of Michigan's DTE utility,

are explored. Note that the proposed methodology utilizes the SEI layer growth and lithium plating mechanisms for battery degradation prediction to demonstrate the idea of its implementation in the performance estimation of second-life batteries. More complex mechanisms, i.e., the particle cracking model, loss of active material model, and the coupling of these mechanisms, could be employed to further improve the estimation accuracy. This methodology offers an appropriate framework for the analysis of the second-life battery in grid applications. It could be extended further for electric grid systems with photovoltaic panels and wind turbines. Moreover, combined with detailed cost estimation approaches for the battery, i.e., replacement and depreciation models, a more comprehensive computational framework could be developed for the revenue optimization of the electric grid system.

Author Contributions: Writing—original draft, R.L.; Grid Optimization, A.H.; Governing Equations of Battery, N.G.; Supervision, W.S. and X.Z. All authors have read and agreed to the published version of the manuscript.

Funding: This research was funded by the Research Initiation & Development Grant (FY23 Winter Cycle) of the University of Michigan—Dearborn Office of Research.

Data Availability Statement: The data are available from the corresponding author upon reasonable request.

Acknowledgments: We are grateful to acknowledge the comments and suggestions from the editor and reviewers for their help in improving the quality of this paper.

Conflicts of Interest: The authors declare no conflict of interest.

References

1. Skeete, J.P.; Wells, P.; Dong, X.; Heidrich, O.; Harper, G. Beyond the EVent Horizon: Battery Waste, Recycling, and Sustainability in the United Kingdom Electric Vehicle Transition. *Energy Res. Soc. Sci.* **2020**, *69*, 101581. [CrossRef]
2. Wang, L.; Wang, X.; Yang, W. Optimal Design of Electric Vehicle Battery Recycling Network—From the Perspective of Electric Vehicle Manufacturers. *Appl. Energy* **2020**, *275*, 115328. [CrossRef]
3. Ioakimidis, C.S.; Murillo-Marrodán, A.; Bagheri, A.; Thomas, D.; Genikomsakis, K.N. Life Cycle Assessment of a Lithium Iron Phosphate (LFP) Electric Vehicle Battery in Second Life Application Scenarios. *Sustainability* **2019**, *11*, 2527. [CrossRef]
4. Hua, Y.; Liu, X.; Zhou, S.; Huang, Y.; Ling, H.; Yang, S. Toward Sustainable Reuse of Retired Lithium-Ion Batteries from Electric Vehicles. *Resour. Conserv. Recycl.* **2021**, *168*, 105249. [CrossRef]
5. Hua, Y.; Zhou, S.; Huang, Y.; Liu, X.; Ling, H.; Zhou, X.; Zhang, C.; Yang, S. Sustainable Value Chain of Retired Lithium-Ion Batteries for Electric Vehicles. *J. Power Sources* **2020**, *478*, 228753. [CrossRef]
6. Chen, W.; Liang, J.; Yang, Z.; Li, G. A Review of Lithium-Ion Battery for Electric Vehicle Applications and Beyond. *Energy Procedia* **2019**, *158*, 4363–4368. [CrossRef]
7. Haram, M.H.S.M.; Lee, J.W.; Ramasamy, G.; Ngu, E.E.; Thiagarajah, S.P.; Lee, Y.H. Feasibility of Utilising Second Life EV Batteries: Applications, Lifespan, Economics, Environmental Impact, Assessment, and Challenges. *Alex. Eng. J.* **2021**, *60*, 4517–4536. [CrossRef]
8. White, C.; Thompson, B.; Swan, L.G. Repurposed Electric Vehicle Battery Performance in Second-Life Electricity Grid Frequency Regulation Service. *J. Energy Storage* **2020**, *28*, 101278. [CrossRef]
9. Sahoo, S.; Timmann, P. Energy Storage Technologies for Modern Power Systems: A Detailed Analysis of Functionalities, Potentials, and Impacts. *IEEE Access* **2023**, *11*, 49689–49729. [CrossRef]
10. Fitzgerald, G.; Mandel, J.; Morris, J.; Touati, H. *The Economics of Battery Energy Storage How Multi-Use, Customer-Sited Batteries Deliver the Most Services and Value to Customers and the Grid the Economics of Battery Energy Storage*; Rocky Mountain Institute: Snowmass, CO, USA, 2015.
11. Aaslid, P.; Korpas, M.; Belsnes, M.M.; Fosso, O.B. Stochastic Optimization of Microgrid Operation With Renewable Generation and Energy Storages. *IEEE Trans. Sustain. Energy* **2022**, *13*, 1481–1491. [CrossRef]
12. Gu, B.; Mao, C.; Liu, B.; Wang, D.; Fan, H.; Zhu, J.; Sang, Z. Optimal Charge/Discharge Scheduling for Batteries in Energy Router-Based Microgrids of Prosumers via Peer-to-Peer Trading. *IEEE Trans. Sustain. Energy* **2022**, *13*, 1315–1328. [CrossRef]
13. Wu, X.; Zhao, J.; Conejo, A.J. Optimal Battery Sizing for Frequency Regulation and Energy Arbitrage. *IEEE Trans. Power Deliv.* **2022**, *37*, 2016–2023. [CrossRef]
14. Hassan, A.; Altin, M.; Bingöl, F. Inertia and Droop Controller for a Modern Variable Speed Wind Turbine to Provide Frequency Control in a Microgrid. *Politek. Derg.* **2020**, *23*, 771–777. [CrossRef]

15. Guan, M. Scheduled Power Control and Autonomous Energy Control of Grid-Connected Energy Storage System (ESS) with Virtual Synchronous Generator and Primary Frequency Regulation Capabilities. *IEEE Trans. Power Syst.* **2022**, *37*, 942–954. [CrossRef]
16. Hassan, A. Frequency Control in an Isolated Power System with High Penetration of Wind Power. Ph.D. Thesis, Izmir Institute of Technology, İzmir, Turkey, 2019.
17. Li, X.; Wang, L.; Yan, N.; Ma, R. Cooperative Dispatch of Distributed Energy Storage in Distribution Network with PV Generation Systems. *IEEE Trans. Appl. Supercond.* **2021**, *31*, 1–4. [CrossRef]
18. Argiolas, L.; Stecca, M.; Elizondo, L.R.; Soeiro, T.B.; Bauer, P. Optimal Battery Energy Storage Dispatch in Energy and Frequency Regulation Markets While Peak Shaving an EV Fast Charging Station. *IEEE Open Access J. Power Energy* **2022**, *9*, 374–385. [CrossRef]
19. Li, X.; Cao, X.; Li, C.; Yang, B.; Cong, M.; Chen, D. A Coordinated Peak Shaving Strategy Using Neural Network for Discretely Adjustable Energy-Intensive Load and Battery Energy Storage. *IEEE Access* **2020**, *8*, 5331–5338. [CrossRef]
20. Rasool, S.; Muttaqi, K.M.; Sutanto, D. A Multi-Filter Based Dynamic Power Sharing Control for a Hybrid Energy Storage System Integrated to a Wave Energy Converter for Output Power Smoothing. *IEEE Trans. Sustain. Energy* **2022**, *13*, 1693–1706. [CrossRef]
21. Fan, F.; Kockar, I.; Xu, H.; Li, J. Scheduling Framework Using Dynamic Optimal Power Flow for Battery Energy Storage Systems. *CSEE J. Power Energy Syst.* **2022**, *8*, 271–280. [CrossRef]
22. Abdalla, A.A.; El Moursi, M.S.; El-Fouly, T.H.M.; Al Hosani, K.H. A Novel Adaptive Power Smoothing Approach for PV Power Plant with Hybrid Energy Storage System. *IEEE Trans. Sustain. Energy* **2023**, *14*, 1457–1473. [CrossRef]
23. Europe's Largest Energy Storage System Now Live at the Johan Cruijff Arena. Available online: https://global.nissannews.com/en/releases/europes-largest-energy-storage-system-now-live-at-the-johan-cruijff-arena (accessed on 15 April 2021).
24. Schimpe, M.; Piesch, C.; Hesse, H.C.; Paß, J.; Ritter, S.; Jossen, A. Power Flow Distribution Strategy for Improved Power Electronics Energy Efficiency in Battery Storage Systems: Development and Implementation in a Utility-Scale System. *Energies* **2018**, *11*, 533. [CrossRef]
25. Second Life Energy Storage: VHH and MAN Testing Use of Second Life of Batteries for EBus Charging Station. Available online: https://press.mantruckandbus.com/second-life-energy-storage-vhh-and-man-testing-use-of-secondlife-of-batteries-for-ebus-charging-station (accessed on 30 June 2020).
26. Chen, Z.; Chen, L.; Shen, W.; Xu, K. Remaining Useful Life Prediction of Lithium-Ion Battery via a Sequence Decomposition and Deep Learning Integrated Approach. *IEEE Trans. Veh. Technol.* **2022**, *71*, 1466–1479. [CrossRef]
27. Cui, X.; Ramyar, A.; Contreras, V.; Judge, G.; Siegel, J.; Stefanopoulou, A.; Avestruz, A.T. Lite-Sparse Hierarchical Partial Power Processing for Parallel Batteries in Heterogeneous Energy Storage Systems. In Proceedings of the 2021 IEEE 22nd Workshop on Control and Modelling of Power Electronics, COMPEL 2021, Cartegena, Colombia, 2–5 November 2021; Institute of Electrical and Electronics Engineers Inc.: New York, NY, USA, 2021.
28. Li, S.; Zhao, P.; Gu, C.; Li, J.; Huo, D.; Cheng, S. Aging Mitigation for Battery Energy Storage System in Electric Vehicles. *IEEE Trans. Smart Grid* **2023**, *14*, 2152–2163. [CrossRef]
29. Fan, F.; Xu, Y.; Zhang, R.; Wan, T. Whole-Lifetime Coordinated Service Strategy for Battery Energy Storage System Considering Multi-Stage Battery Aging Characteristics. *J. Mod. Power Syst. Clean Energy* **2022**, *10*, 689–699. [CrossRef]
30. Zhang, L.; Yu, Y.; Li, B.; Qian, X.; Zhang, S.; Wang, X.; Zhang, X.; Chen, M. Improved Cycle Aging Cost Model for Battery Energy Storage Systems Considering More Accurate Battery Life Degradation. *IEEE Access* **2022**, *10*, 297–307. [CrossRef]
31. Janota, L.; Králík, T.; Knápek, J. Second Life Batteries Used in Energy Storage for Frequency Containment Reserve Service. *Energies* **2020**, *13*, 6396. [CrossRef]
32. Steckel, T.; Kendall, A.; Ambrose, H. Applying Levelized Cost of Storage Methodology to Utility-Scale Second-Life Lithium-Ion Battery Energy Storage Systems. *Appl. Energy* **2021**, *300*, 117309. [CrossRef]
33. Wang, B.; Ji, C.; Wang, S.; Sun, J.; Pan, S.; Wang, D.; Liang, C. Study of Non-Uniform Temperature and Discharging Distribution for Lithium-Ion Battery Modules in Series and Parallel Connection. *Appl. Therm. Eng.* **2020**, *168*, 114831. [CrossRef]
34. Wang, Y.; Tian, J.; Sun, Z.; Wang, L.; Xu, R.; Li, M.; Chen, Z. A Comprehensive Review of Battery Modeling and State Estimation Approaches for Advanced Battery Management Systems. *Renew. Sustain. Energy Rev.* **2020**, *131*, 110015. [CrossRef]
35. Zhang, Q.; Wang, D.; Yang, B.; Cui, X.; Li, X. Electrochemical Model of Lithium-Ion Battery for Wide Frequency Range Applications. *Electrochim. Acta* **2020**, *343*, 136094. [CrossRef]
36. Nejad, S.; Gladwin, D.T.; Stone, D.A. A Systematic Review of Lumped-Parameter Equivalent Circuit Models for Real-Time Estimation of Lithium-Ion Battery States. *J. Power Sources* **2016**, *316*, 183–196. [CrossRef]
37. Seaman, A.; Dao, T.S.; McPhee, J. A Survey of Mathematics-Based Equivalent-Circuit and Electrochemical Battery Models for Hybrid and Electric Vehicle Simulation. *J. Power Sources* **2014**, *256*, 410–423. [CrossRef]
38. Wang, Y.; Yang, D.; Zhang, X.; Chen, Z. Probability Based Remaining Capacity Estimation Using Data-Driven and Neural Network Model. *J. Power Sources* **2016**, *315*, 199–208. [CrossRef]
39. Wei, J.; Dong, G.; Chen, Z. Remaining Useful Life Prediction and State of Health Diagnosis for Lithium-Ion Batteries Using Particle Filter and Support Vector Regression. *IEEE Trans. Ind. Electron.* **2018**, *65*, 5634–5643. [CrossRef]
40. Doyle, M.; Fuller, T.; Newman, J. Modeling of Galvanostatic Charge and Discharge of the Lithium/Polymer/Insertion Cell. *J. Electrochem. Soc.* **1993**, *140*, 1526–1533. [CrossRef]

41. Dao, T.S.; Vyasarayani, C.P.; McPhee, J. Simplification and Order Reduction of Lithium-Ion Battery Model Based on Porous-Electrode Theory. *J. Power Sources* **2012**, *198*, 329–337. [CrossRef]
42. Han, X.; Ouyang, M.; Lu, L.; Li, J. Simplification of Physics-Based Electrochemical Model for Lithium Ion Battery on Electric Vehicle. Part II: Pseudo-Two-Dimensional Model Simplification and State of Charge Estimation. *J. Power Sources* **2015**, *278*, 814–825. [CrossRef]
43. Xu, M.; Wang, R.; Zhao, P.; Wang, X. Fast Charging Optimization for Lithium-Ion Batteries Based on Dynamic Programming Algorithm and Electrochemical-Thermal-Capacity Fade Coupled Model. *J. Power Sources* **2019**, *438*, 227015. [CrossRef]
44. Song, X.; Lu, Y.; Wang, F.; Zhao, X.; Chen, H. A Coupled Electro-Chemo-Mechanical Model for All-Solid-State Thin Film Li-Ion Batteries: The Effects of Bending on Battery Performances. *J Power Sources* **2020**, *452*, 227803. [CrossRef]
45. Cai, L.; White, R.E. Mathematical Modeling of a Lithium Ion Battery with Thermal Effects in COMSOL Inc. Multiphysics (MP) Software. *J. Power Sources* **2011**, *196*, 5985–5989. [CrossRef]
46. FORTRAN Programs for the Simulation of Electrochemical Systems. Available online: http://www.cchem.berkeley.edu/jsngrp/fortran.html (accessed on 15 July 2023).
47. Torchio, M.; Magni, L.; Gopaluni, R.B.; Braatz, R.D.; Raimondo, D.M. LIONSIMBA: A Matlab Framework Based on a Finite Volume Model Suitable for Li-Ion Battery Design, Simulation, and Control. *J. Electrochem. Soc.* **2016**, *163*, A1192–A1205. [CrossRef]
48. Sulzer, V.; Marquis, S.G.; Timms, R.; Robinson, M.; Chapman, S.J. Python Battery Mathematical Modelling (PyBaMM). *J. Open Res. Softw.* **2021**, *9*, 14. [CrossRef]
49. Safari, M.; Morcrette, M.; Teyssot, A.; Delacourt, C. Multimodal Physics-Based Aging Model for Life Prediction of Li-Ion Batteries. *J. Electrochem. Soc.* **2009**, *156*, A145. [CrossRef]
50. Single, F.; Latz, A.; Horstmann, B. Identifying the Mechanism of Continued Growth of the Solid–Electrolyte Interphase. *ChemSusChem* **2018**, *11*, 1950–1955. [CrossRef] [PubMed]
51. Luo, G.; Zhang, Y.; Tang, A. Capacity Degradation and Aging Mechanisms Evolution of Lithium-Ion Batteries under Different Operation Conditions. *Energies* **2023**, *16*, 4232. [CrossRef]
52. O'Kane, S.E.J.; Ai, W.; Madabattula, G.; Alonso-Alvarez, D.; Timms, R.; Sulzer, V.; Edge, J.S.; Wu, B.; Offer, G.J.; Marinescu, M. Lithium-Ion Battery Degradation: How to Model It. *Phys. Chem. Chem. Phys.* **2022**, *24*, 7909–7922. [CrossRef]
53. Doyle, M.; Newman, J. Comparison of Modeling Predictions with Experimental Data from Plastic Lithium Ion Cells. *J. Electrochem. Soc.* **1996**, *143*, 1890–1903. [CrossRef]
54. Plett, G.L. *Battery Management Systems, Volume I: Battery Modeling*; Artech House: London, UK, 2015; Volume 1, p. 343.
55. Marquis, S.G. Long-Term Degradation of Lithium-Ion Batteries. Ph.D. Thesis, University of Oxford, Oxford, UK, 2020.
56. Chen, C.-H.; Brosa Planella, F.; O'Regan, K.; Gastol, D.; Widanage, W.D.; Kendrick, E. Development of Experimental Techniques for Parameterization of Multi-Scale Lithium-Ion Battery Models. *J. Electrochem. Soc.* **2020**, *167*, 080534. [CrossRef]